DOE/ET/53088/85 IFSR #85

VARIATIONAL METHOD FOR THE THREE-DIMENSIONAL INVERSE EQUILIBRIUM PROBLEM IN TOROIDS: PART 2

A. Bhattacharjee,
Institute for Fusion Studies

J. C. Wiley,
Fusion Research Center
The University of Texas at Austin

and R. L. Dewar
Research School of Physical Sciences
The Australian National University

May 1983

VARIATIONAL METHOD FOR THE THREE-DIMENSIONAL INVERSE EQUILBRIUM PROBLEM IN TOROIDS: PART TWO

A. Bhattacharjee,
Institute for Fusion Studies
The University of Texas at Austin
Austin, Texas 78712 USA
and
Plasma Physics Programme
Physical Research Laboratory
Ahmedabad 380009, India

J. C. Wiley,
Fusion Research Center
The University of Texas at Austin
Austin, Texas 78712

and

R. L. Dewar,
Research School of Physical Sciences
The Australian National University
Canberra ACT 2600, Australia

Abstract

A variational method, which has been recently proposed for computing the inverse solutions for three-dimensional magnetostatic equilibria, is generalized to allow for variations in the magnetic toroidal angle. It is found that the procedure improves the accuracy and convergence properties of the method.

I. INTRODUCTION

Recently, we have developed a variational method[1] for computing three-dimensional, magnetostatic equilibria in toroids. In this method, equilibria are represented by the inverse mapping

$$R = R(v,\theta,\zeta) \tag{1a}$$

$$\phi = \phi(v,\theta,\zeta) \tag{1b}$$

$$Z = Z(v,\theta,\zeta) \tag{1c}$$

where (R,ϕ,Z) define a cylindrical coordinate system, and (v,θ,ζ) a magnetic coordinate system, with the magnetic field $\underset{\sim}{B}$ given by

$$\underset{\sim}{B} = \underset{\sim}{\nabla}\zeta \times \underset{\sim}{\nabla}\Psi(v) + \underset{\sim}{\nabla}\Phi(v) \times \underset{\sim}{\nabla}\theta \quad . \tag{2}$$

In the representation for $\underset{\sim}{B}$ written above, referred to often as the "straight field-line" form, v is any radial flux surface label, and θ and ζ are, respectively, the poloidal and toroidal angles parameterizing a flux surface. The poloidal flux function Ψ and the toroidal flux function Φ are both surface quantities. The essence of our method is to Fourier-expand the inverse variables in θ and ζ, and derive from the variational principle due to Grad[2] (or Kruskal and Kulsrud[3]) a set of ordinary differential equations for the amplitudes in v. A fully three-dimensional problem is thus reduced to a one-dimensional problem.

It was pointed out in our earlier paper that if $\underset{\sim}{B}$ is represented by Eq. (2), there is a degree of freedom in the construction of the angles θ and ζ. We may choose one of these angles, but the other

angle is then determined by the variational principle, so that the magnetic field lines are straight in (θ,ζ) space. In our earlier work, we chose

$$\zeta = \phi \quad , \tag{3}$$

and θ is consequently determined by the variational principle. The rationale for making the above choice is that it reduces not only the number of equations to be solved, but also the degree of nonlinearity of each equation. However, there is a price to be paid for this simple choice. Since the shape of the outermost flux surface is to be held fixed during the process of iteration, but θ is not known ahead of time, we are required to iterate on the Fourier amplitudes initially chosen to parameterize the outermost surface. Our experience has indicated that under these conditions, the convergence properties of the method are not entirely satisfactory.

The hint for a more satisfying resolution of the problem is already evident in our earlier paper[1] if we note that on the outermost surface we essentially solve moments of the equation

$$\underset{\sim}{J}\cdot\underset{\sim}{\nabla}v = 0 \quad , \tag{4}$$

where $\underset{\sim}{J}$ is the current density. We recall now that Eq. (4) may be derived from the variational principle if we allow either θ or ζ to vary. In order to circumvent the problems associated with iterating on the boundary, we now specify θ , and the magnetic toroidal angle ζ is allowed to vary so as to keep field lines straight in (θ,ζ) space. This is achieved by defining

$$\zeta \equiv \phi - q(v)\Lambda(v,\theta,\zeta) , \tag{5}$$

where $\Lambda(v,\theta,\zeta)$ is a periodic function in θ and ζ, and $q(v)$ is the safety factor. Like R and Z, Λ is expanded in a Fourier series in θ and ζ, and the variational principle is used to obtain ordinary differential equations for the amplitudes in v.

Equation (15) generalizes for three-dimensional equilibria the definition of the toroidal angle used by Grimm, Dewar, and Manickam[4] for axisymmetric systems. The procedure of varying the toroidal angle ζ, which is a natural extension of our earlier work, is equivalent to the procedure used by Bauer, Betancourt, and Garabedian[5], and more recently, by Hirshman and Whitson.[6] It has the attractive feature that the equilibrium constraint embodied by Eq. (4) is satisfied throughout the plasma volume at every step of the iteration process.

The plan of the paper is as follows. In Sec. II, we describe the variational principle and derive the relevant Euler-Lagrange equations. In Sec. III, we expand R, Z, and Λ in Fourier series and derive from the variational principle Euler-Lagrange equations for the amplitudes in v. In Sec. IV, we explain our choice of the radial label, the boundary conditions, and explain the modifications necessary in our earlier code in order to accommodate variation of ζ. In Sec. V, we report comparisons with the analytic Solov́ev equilibria used to benchmark the earlier version of our code, and numerical results on three-dimensional stellarator equilibria.

II. VARIATIONAL PRINCIPLE

It has been shown[1,2] that the first variation of the functional

$$L = \int_{V_0} d\tau \left(\frac{B^2}{2} - p \right) , \tag{6}$$

defined over the total volume V_0 of a toroidal plasma bounded by a perfectly conducting wall, with $\underset{\sim}{B}$ represented by Eq. (2) and pressure $p = p(v)$, vanishes if, and only if, the magnetostatic equations are satisfied. Treating $R(v,\theta,\zeta)$, $Z(v,\theta,\zeta)$ and $\Lambda(v,\theta,\zeta)$ as dependent variables, we write L in the form

$$L \equiv \int_0^a dv \int_0^{2\pi} d\theta \int_0^{2\pi} d\zeta \; \mathscr{L}(R, R_v, R_\theta, R_\zeta, Z_v, Z_\theta, Z_\zeta, \Lambda_\theta, \Lambda_\zeta) ,$$

$$= \int_0^a dv \int_0^{2\pi} d\theta \int_0^{2\pi} d\zeta \; \sqrt{\| g \|} \left(\frac{\alpha_v^2}{2} \frac{g_{\theta\theta}}{\| g \|} + \frac{\beta_v^2}{2} \frac{g_{\zeta\zeta}}{\| g \|} + \alpha_v \beta_v \frac{g_{\theta\zeta}}{\| g \|} - p \right) , \tag{7}$$

where

$$\alpha_v \equiv \Psi_v (1 - q\Lambda_\zeta) , \tag{8a}$$

and

$$\beta_v \equiv \Phi_v (1 + \Lambda_\theta) . \tag{8b}$$

The elements of the metric tensor g_{ij} are given by

$$g_{vv} = R_v^2 + Z_v^2 , \tag{9a}$$

$$g_{v\theta} = R_v R_\theta + Z_v Z_\theta = g_{\theta v} \quad , \tag{9b}$$

$$g_{\zeta v} = R_\zeta R_v + Z_\zeta Z_v = g_{v\zeta} \quad , \tag{9c}$$

$$g_{\theta\theta} = R_\theta^2 + Z_\theta^2 \quad , \tag{9d}$$

$$g_{\theta\zeta} = R_\theta R_\zeta + Z_\theta Z_\zeta = g_{\zeta\theta} \quad , \tag{9e}$$

$$g_{\zeta\zeta} = R^2 + R_\zeta^2 + Z_\zeta^2 \quad , \tag{9f}$$

and the Jacobian

$$\sqrt{\| g \|} = R(R_\theta Z_v - R_v Z_\theta) \ . \tag{10}$$

Two comments are in order. First, the form of $\mathscr{L}$ given by Eq. (7) is identical to the form given in Ref. 1 if we replace α_v by Ψ_v, and β_v by Φ_v. This observation helps us carry over most of the algebraic manipulations in Ref. 1 easily. Second, $\mathscr{L}$ is independent of Λ_v. The Euler-Lagrange equation for Λ is therefore expected to be independent of Λ_v, and may be solved within each magnetic surface.

The first variation of L gives, in the manner shown in Ref. 1, the following Euler-Lagrange equations for variations with respect to R, Z, and Λ respectively:

$$Q_1 \equiv \left(RZ_\theta \frac{\partial}{\partial v} - RZ_v \frac{\partial}{\partial \theta}\right)\left(\frac{\alpha_v^2}{2}\frac{g_{\theta\theta}}{\|g\|} + \frac{\beta_v^2}{2}\frac{g_{\zeta\zeta}}{\|g\|} + \alpha_v\beta_v\frac{g_{\theta\zeta}}{\|g\|} + p'\right)$$

$$+ \alpha_v^2 \frac{\partial}{\partial\theta}\frac{R_\theta}{\sqrt{\|g\|}} + \beta_v^2\left(\frac{\partial}{\partial\zeta}\frac{R_\zeta}{\sqrt{\|g\|}} - \frac{R}{\sqrt{\|g\|}}\right) + \alpha_v\beta_v\left(\frac{\partial}{\partial\theta}\frac{R_\zeta}{\sqrt{\|g\|}} + \frac{\partial}{\partial\zeta}\frac{R_\theta}{\sqrt{\|g\|}}\right)$$

$$= 0 \qquad (11)$$

$$Q_3 \equiv \left(-RR_\theta \frac{\partial}{\partial v} + RR_v \frac{\partial}{\partial \theta}\right)\left(\frac{\alpha_v^2}{2}\frac{g_{\theta\theta}}{\|g\|} + \frac{\beta_v^2}{2}\frac{g_{\zeta\zeta}}{\|g\|} + \alpha_v\beta_v\frac{g_{\theta\zeta}}{\|g\|} + p'\right)$$

$$+ \alpha_v^2 \frac{\partial}{\partial\theta}\frac{Z_\theta}{\sqrt{\|g\|}} + \beta_v^2\frac{\partial}{\partial\zeta}\frac{Z_\zeta}{\sqrt{\|g\|}} + \alpha_v\beta_v\left(\frac{\partial}{\partial\theta}\frac{Z_\zeta}{\sqrt{\|g\|}} + \frac{\partial}{\partial\zeta}\frac{Z_\theta}{\sqrt{\|g\|}}\right) = 0 \ , \qquad (12)$$

and

$$Q_0 \equiv \frac{\partial}{\partial\theta}\left\{\frac{\Phi_v}{\sqrt{\|g\|}}\left[g_{\zeta\zeta}(\Lambda_\theta + 1) - g_{\theta\zeta}\Lambda_\zeta\right] + \frac{\Psi_v}{\sqrt{\|g\|}}g_{\theta\zeta}\right\}$$

$$- \frac{\partial}{\partial\zeta}\left\{\frac{\Phi_v}{\sqrt{\|g\|}}\left[g_{\theta\zeta}(\Lambda_\theta + 1) - g_{\theta\theta}\Lambda_\zeta\right] + \frac{\Psi_v}{\sqrt{\|g\|}}g_{\theta\theta}\right\} = 0 \ . \qquad (13)$$

Equations (11), (12) and (13) may be identified to be

$$\underset{\sim}{\nabla}R\cdot\underset{\sim}{\nabla}\left(\frac{B^2}{2} + p\right) - \underset{\sim}{B}\cdot\underset{\sim}{\nabla}B_R - \frac{B_\phi^2}{R} = 0 \ , \qquad (14)$$

$$\underset{\sim}{\nabla}Z\cdot\underset{\sim}{\nabla}\left(\frac{B^2}{2} + p\right) - \underset{\sim}{B}\cdot\underset{\sim}{\nabla}(B_Z) = 0 \ , \qquad (15)$$

and

$$\underset{\sim}{J}\cdot\underset{\sim}{\nabla}v = \underset{\sim}{\nabla}\cdot(\underset{\sim}{B}\times\underset{\sim}{\nabla}v) = 0 \quad , \tag{16}$$

respectively, where

$$B_R \equiv \underset{\sim}{B}\cdot\underset{\sim}{\nabla}R \quad , \tag{17a}$$

$$B_\phi \equiv R\underset{\sim}{B}\cdot\underset{\sim}{\nabla}\phi \quad , \tag{17b}$$

and

$$B_Z \equiv \underset{\sim}{B}\cdot\underset{\sim}{\nabla}Z \quad . \tag{17c}$$

Equations (14) and (15) are, respectively, the covariant components in the $\underset{\sim}{\nabla}R$ and $\underset{\sim}{\nabla}Z$ directions of $\underset{\sim}{J}\times\underset{\sim}{B} = \underset{\sim}{\nabla}p$, which may be written in the form

$$\underset{\sim}{\nabla}\left(\frac{B^2}{2} + p\right) - \underset{\sim}{B}\cdot\underset{\sim}{\nabla}\underset{\sim}{B} = 0 \quad . \tag{18}$$

As pointed out in Ref. 1, the covariant component of Eq. (18) in the $\underset{\sim}{\nabla}\phi$ direction,

$$R\underset{\sim}{\nabla}\phi\cdot\underset{\sim}{\nabla}\left(\frac{B^2}{2} + p\right) - \underset{\sim}{B}\cdot\underset{\sim}{\nabla}(RB_\phi) = 0 \tag{19}$$

---

may be shown to be a consequence of Eqs. (14), (15) and (16) and is not an independent equation.

Before we conclude this section, we write for future reference, $\underset{\sim}{J}\times\underset{\sim}{B} = p_v\underset{\sim}{\nabla}v$, in terms of inverse variables R and Z , and Λ :

$$Q \equiv \frac{\alpha_v}{\sqrt{\|g\|}}\left[\frac{\partial}{\partial v}\left(\frac{\alpha_v g_{\theta\theta}}{\sqrt{\|g\|}} + \frac{\beta_v g_{\theta\zeta}}{\sqrt{\|g\|}}\right) - \frac{\partial}{\partial\theta}\left(\frac{\alpha_v g_{v\theta}}{\sqrt{\|g\|}} + \frac{\beta_v g_{\zeta v}}{\sqrt{\|g\|}}\right)\right]$$

$$+ \frac{\beta_v}{\sqrt{\|g\|}}\left[\frac{\partial}{\partial v}\left(\frac{\alpha_v g_{\theta\zeta}}{\sqrt{\|g\|}} + \frac{\beta_v g_{\zeta\zeta}}{\sqrt{\|g\|}}\right) - \frac{\partial}{\partial\zeta}\left(\frac{\alpha_v g_{v\theta}}{\sqrt{\|g\|}} + \frac{\beta_v g_{\zeta v}}{\sqrt{\|g\|}}\right)\right] + p_v = 0 \quad . \tag{20}$$

III. EULER-LAGRANGE EQUATIONS FOR FOURIER AMPLITUDES

Exploiting the periodicity of $R(v,\theta,\zeta)$, $Z(v,\theta,\zeta)$ and $\Lambda(v,\theta,\zeta)$ in θ and ζ , we expand them in Fourier series.

$$R(v,\theta,\zeta) = \sum\left[R_{m_1,m_2}(v)\cos(m_1\theta - m_2\zeta) + R_{n_1,n_2}(v)\sin(n_1\theta - n_2\zeta)\right] \tag{21}$$

$$Z(v,\theta,\zeta) = \sum\left[Z_{p_1,p_2}(v)\cos(p_1\theta - p_2\zeta) + Z_{q_1,q_2}(v)\sin(q_1\theta - q_2\zeta)\right] \tag{22}$$

$$\Lambda(v,\theta,\zeta) = \sum\left[\Lambda_{r_1,r_2}(v)\cos(r_1\theta - r_2\zeta) + \Lambda_{s_1,s_2}(v)\sin(s_1\theta - s_2\zeta)\right] \tag{23}$$

where, unless stated otherwise, the sums extend from $-\infty$ to $+\infty$ over all integers. Substituting series (21) through (23) in L , and varying

each amplitude in v independently, we derive the following infinite set of ordinary differential equations for stationary values of L :

$$\langle\langle \cos(m_1\theta - m_2\zeta)Q_1 \rangle\rangle = 0 \qquad m_1, m_2 \in (-\infty, +\infty) \tag{24a}$$

$$\langle\langle \sin(n_1\theta - n_2\zeta)Q_1 \rangle\rangle = 0 \qquad n_1, n_2 \in (-\infty, +\infty) \tag{24b}$$

$$\langle\langle \cos(p_1\theta - p_2\zeta)Q_3 \rangle\rangle = 0 \qquad p_1, p_2 \in (-\infty, +\infty) \tag{24c}$$

$$\langle\langle \sin(q_1\theta - q_2\zeta)Q_3 \rangle\rangle = 0 \qquad q_1, q_2 \in (-\infty, +\infty) \tag{24d}$$

$$\langle\langle \cos(r_1\theta - r_2\zeta)Q_0 \rangle\rangle = 0 \qquad r_1, r_2 \in (-\infty, +\infty) \tag{24e}$$

$$\langle\langle \sin(s_1\theta - s_2\zeta)Q_0 \rangle\rangle = 0 \qquad s_1, s_2 \in (-\infty, +\infty) \tag{24f}$$

where $\langle\langle\ \rangle\rangle$ is the double-averaging operator, defined by

$$\langle\langle A \rangle\rangle \equiv (2\pi)^{-2} \int_0^{2\pi} d\theta \int_0^{2\pi} d\zeta\ A(v,\theta,\zeta) \quad . \tag{25}$$

In what follows we will consider equilibria which have the symmetry property that if $\theta \to -\theta$ and $\zeta \to -\zeta$, then $R \to R$ and $Z \to -Z$. The above symmetry operations require that $\Lambda \to -\Lambda$. We will, therefore, restrict ourselves to only Eqs. (24a), (24d) and (24f).

IV. CHOICE OF THE RADIAL FLUX SURFACE LABEL AND BOUNDARY CONDITIONS

As pointed out in Ref. 1, any one of the Fourier amplitudes may be used for labelling flux surfaces. The surface-averaged pressure balance equation, given by

$$\langle\langle \sqrt{\|g\|}\, Q \rangle\rangle = 0 \quad , \tag{26}$$

takes the place, formally speaking, of the Euler-Lagrange equation for the Fourier amplitude chosen. Alternatively, we may specify the functional relation between v and Ψ ,

$$v = v(\Psi) \quad . \tag{27}$$

Following the practice of Ref. 1, we continue to use $R_{10} = -|\alpha| v$, where $|\alpha|$ is a positive scaling factor fixed by the geometry of the outermost surface.

One set of boundary conditions for the Fourier amplitudes is obtained by Fourier analyzing the outermost surface at $v = a$. We define

$$R^a_{m_1,m_2} \equiv R_{m_1,m_2}(a) \quad , \tag{28a}$$

$$Z^a_{q_1,q_2} \equiv Z_{q_1,q_2}(a) \quad . \tag{28b}$$

The poloidal flux function Ψ is a constant on the outermost surface, given by

$$\Psi^a \equiv \Psi(a) \quad . \tag{29}$$

Near the axis we impose, as in Ref. 1,

$$R'_{m_1,m_2}(0) = 0 \qquad (m_1 = 0) \quad , \tag{30a}$$

$$R_{m_1,m_2}(0) = 0 \qquad (m_1 \neq 0) \quad , \tag{30b}$$

$$Z'_{q_1,q_2}(0) = 0 \qquad (q_1 = 0) \ , \tag{30c}$$

$$Z_{q_1,q_2}(0) = 0 \qquad (q_1 \neq 0) \ , \tag{30d}$$

where $f' \equiv f_v$.

The boundary condition for Ψ at $v = 0$, necessary in order to pin down the solution to Eq. (20), needs to be handled carefully. In the manner shown in Ref. 1, we transform to a new dependent variable

$$u(v) = \frac{\Psi_v}{v} \ , \tag{31}$$

and use the transformed Eq. (20) to obtain $u(0)$ iteratively. Once u is obtained, we integrate Eq. (31), subject to Eq. (29), to obtain Ψ .

The moment equations for Λ , given by Eq. (24f), have no radial derivatives, and are therefore solved within each surface. The numerical results we present are determined by two given functions, the toroidal field function $F(\Psi)$ and the pressure $p(\Psi)$. In the special case of axisymmetry

$$F = \Phi_v \frac{g_{\zeta\zeta}}{\sqrt{\| g \|}} (1 + \Lambda_\theta) \ . \tag{32}$$

The solubility condition for Λ now gives

$$F = \frac{\Phi_v}{\langle\langle \sqrt{\| g \|} / g_{\zeta\zeta} \rangle\rangle} \ , \tag{33}$$

which is subtly different from the prescription for F in Ref. 1.

Though introduced here in the context of axisymmetry, we carry over the prescription given by Eq. (33) for three-dimensional equilibria. To obtain Φ , we integrate Eq. (33) subject to the condition

$$\Phi(0) = 0 \quad . \tag{34}$$

In summary, we solve numerically Eqs. (24a), (24d), (24f), (26) and (33), subject to the stated boundary conditions, by the method of collocation at Gaussian points due to DeBoor and Swartz.[7] For a detailed explanation, the reader is referred to Ref. 1. We state here only the modification due to the introduction of Λ in the formalism. The moment equations for Λ , given by Eq. (24f), have no radial derivatives, and are therefore solved within each surface at every step of the iteration process. This may not be the most computationally efficient strategy, because it does not sufficiently exploit the fact that Q_0 is a linear, Poisson-like equation in Λ . However, we have adopted it because it was the easiest one to implement within the existing framework of our earlier code.

V. NUMERICAL RESULTS

We first compare the numerical results with the analytic, axisymmetric Solov'ev equilibrium used as a test case in Ref. 1. The outermost surface is described by the parametric equations

$$R(v=a,\theta) = R^a_{00} - |\alpha|\cos\theta + R^a_{20}\cos 2\theta + R^a_{30}\cos 3\theta \tag{35a}$$

and

$$Z(v=a,\theta) = Z^a_{10}\sin\theta + Z^a_{20}\sin 2\theta + Z^a_{30}\sin 3\theta \qquad (35b)$$

where $R^a_{00} = 3.881$, $|\alpha| = 1.036$, $R^a_{20} = -0.0172$, $R^a_{30} = 1.8\times 10^{-4}$, $Z^a_{10} = 1.569$, $Z^a_{20} = 0.0807$, and $Z^a_{30} = -3.89\times 10^{-3}$. In Fig. 1, we show the flux surface contours on any poloidal section of the torus. In Fig. 2, we show the radial profiles of the dominant Fourier amplitudes. On comparison with the analogous plot in Ref. 1, we no longer observe the "boundary-layer" effect, noticable, for example, in R_{00} R_{30} , and Z_{30} of Fig. 3 in Ref. 1.

In Table I, we compare the error in Ψ (defined to be $\max|\Psi^N - \Psi|/\Psi^a$, where Ψ^N and Ψ are respectively the numerical and exact values of Ψ as we increase the number of splines (or collocation points), holding all other parameters fixed. There is considerable improvement over our earlier results not only in the absolute magnitude of the error, but more importantly, in the rate of convergence.

We now present numerical results on the three-dimensional equilibria reported in Ref. 1. For the first case, the outermost surface is given by

$$R = R^a_{00} - |\alpha|\cos\theta + R^a_{20}\cos 2\theta + R^a_{11}\cos(\theta - \zeta) \qquad (36a)$$

$$Z = Z^a_{10}\sin\theta + Z^a_{20}\sin 2\theta + Z^a_{11}\sin(\theta - \zeta) \ , \qquad (36b)$$

where R^a_{00} , $|\alpha|$, R^a_{20} , Z^a_{10} , and Z^a_{20} have the same numerical values as Eqs. (35), and $R^a_{11} = Z^a_{11} = 0.333$. In Fig. 4, we show the flux surface contours on different poloidal planes along the axis and in

Fig. 5 the radial profiles of the dominant Fourier amplitudes. The magnetic axis for this equilibrium lies almost entirely in a plane.

We then consider a three-dimensional equilibrium with a spatial magnetic axis. The outermost surface is described by

$$R = R^a_{00} - |\alpha|\cos\theta + R^a_{20}\cos 2\theta + R^a_{01}\cos\zeta \qquad (37a)$$

$$Z = Z^a_{10}\sin\theta + Z^a_{20}\sin 2\theta + Z^a_{01}\sin\zeta \quad , \qquad (37b)$$

where once again R^a_{00} , $|\alpha|$, R^a_{20} , Z^a_{10} , and Z^a_{20} have the same numerical values as before and $R^a_{01} = Z^a_{01} = 0.333$. In Fig. 6, we show the flux surface contours, and in Fig. 7, the radial profiles for the dominant Fourier amplitudes.

In all the numerical results reported, we have used single precision arithmetic on a VAX-11/780 computer. The residuals for the equations solved numerically were in the range 10^{-4} - 10^{-7} for the solutions presented at the termination of the computer runs.

Acknowledgments

The first author (A.B.) would like to thank Ms. K. S. Al-Sweilem for typing this manuscript at short notice. This work was supported primarily by the United States Department of Energy under contract no. DE-FG05-80ET-53088 with the Institute for Fusion Studies and contract no. DE-AC05-79ET-53036 with the Fusion Research Center.

References

1. A. Bhattacharjee, J. C. Wiley, and R. L. Dewar, Institute for Fusion Studies Report IFSR#48-R (University of Texas, Austin, 1983).

2. H. Grad, Phys. Fluids 7, 1283 (1964).

3. M. D. Kruskal and R. M. Kulsrud, Phys. Fluids 1, 265 (1958).

4. R. C. Grimm, R. L. Dewar, and J. Manickam, PPPL-1885 (Princeton Plasma Physics Laboratory, New Jersey, 1982).

5. F. Bauer, O. Betancourt, and P. Garabedian, A Computational Method in Plasma Physics (Springer-Verlag, New York, 1978).

6. S. P. Hirshman and J. C. Whitson, Proceedings of the 1983 Sherwood Theory Meeting, March 21-23, 1983 in Arlington, Va., Paper 3A3.

Figure Captions

Fig. 1 Flux surfaces for the test Solov́ev equilibrium, projected on a poloidal surface.

Fig. 2 Radial profiles of the dominant Fourier amplitudes for the equilibrium shown in Fig. 1.

Fig. 3 Energy (normalized) versus number of iterations for the test Solov́ev equilibrium.

Fig. 4 Flux contours for a three-dimensional stellarator equilibrium with a planar magnetic axis.

Fig. 5 Radial profiles of the dominant Fourier amplitudes for the equilibrium shown in Fig. 4.

Fig. 6 Flux surface contours for a three-dimensional stellarator equilibrium with a spatial magnetic axis.

Fig. 7 Radial profiles of the dominant fourier amplitudes for the equilibrium shown in Fig. 6.

VARIATIONAL METHOD FOR THE THREE-DIMENSIONAL INVERSE EQUILBRIUM PROBLEM IN TOROIDS: PART TWO

A. Bhattacharjee,
Institute for Fusion Studies
The University of Texas at Austin
Austin, Texas 78712 USA
and
Plasma Physics Programme
Physical Research Laboratory
Ahmedabad 380009, India

J. C. Wiley,
Fusion Research Center
The University of Texas at Austin
Austin, Texas 78712

and

R. L. Dewar,
Research School of Physical Sciences
The Australian National University
Canberra ACT 2600, Australia

Abstract

A variational method, which has been recently proposed for computing the inverse solutions for three-dimensional magnetostatic equilibria, is generalized to allow for variations in the magnetic toroidal angle. It is found that the procedure improves the accuracy and convergence properties of the method.

I. INTRODUCTION

Recently, we have developed a variational method[1] for computing three-dimensional, magnetostatic equilibria in toroids. In this method, equilibria are represented by the inverse mapping

$$R = R(v,\theta,\zeta) \tag{1a}$$

$$\phi = \phi(v,\theta,\zeta) \tag{1b}$$

$$Z = Z(v,\theta,\zeta) \tag{1c}$$

where (R,ϕ,Z) define a cylindrical coordinate system, and (v,θ,ζ) a magnetic coordinate system, with the magnetic field $\underset{\sim}{B}$ given by

$$\underset{\sim}{B} = \underset{\sim}{\nabla}\zeta \times \underset{\sim}{\nabla}\Psi(v) + \underset{\sim}{\nabla}\Phi(v) \times \underset{\sim}{\nabla}\theta \quad . \tag{2}$$

In the representation for $\underset{\sim}{B}$ written above, referred to often as the "straight field-line" form, v is any radial flux surface label, and θ and ζ are, respectively, the poloidal and toroidal angles parameterizing a flux surface. The poloidal flux function Ψ and the toroidal flux function Φ are both surface quantities. The essence of our method is to Fourier-expand the inverse variables in θ and ζ, and derive from the variational principle due to Grad[2] (or Kruskal and Kulsrud[3]) a set of ordinary differential equations for the amplitudes in v. A fully three-dimensional problem is thus reduced to a one-dimensional problem.

It was pointed out in our earlier paper that if $\underset{\sim}{B}$ is represented by Eq. (2), there is a degree of freedom in the construction of the angles θ and ζ. We may choose one of these angles, but the other

angle is then determined by the variational principle, so that the magnetic field lines are straight in (θ,ζ) space. In our earlier work, we chose

$$\zeta = \phi \quad , \tag{3}$$

and θ is consequently determined by the variational principle. The rationale for making the above choice is that it reduces not only the number of equations to be solved, but also the degree of nonlinearity of each equation. However, there is a price to be paid for this simple choice. Since the shape of the outermost flux surface is to be held fixed during the process of iteration, but θ is not known ahead of time, we are required to iterate on the Fourier amplitudes initially chosen to parameterize the outermost surface. Our experience has indicated that under these conditions, the convergence properties of the method are not entirely satisfactory.

The hint for a more satisfying resolution of the problem is already evident in our earlier paper[1] if we note that on the outermost surface we essentially solve moments of the equation

$$\underset{\sim}{J}\cdot\underset{\sim}{\nabla}v = 0 \quad , \tag{4}$$

where $\underset{\sim}{J}$ is the current density. We recall now that Eq. (4) may be derived from the variational principle if we allow either θ or ζ to vary. In order to circumvent the problems associated with iterating on the boundary, we now specify θ , and the magnetic toroidal angle ζ is allowed to vary so as to keep field lines straight in (θ,ζ) space. This is achieved by defining

$$\zeta \equiv \phi - q(v)\Lambda(v,\theta,\zeta) , \tag{5}$$

where $\Lambda(v,\theta,\zeta)$ is a periodic function in θ and ζ, and $q(v)$ is the safety factor. Like R and Z, Λ is expanded in a Fourier series in θ and ζ, and the variational principle is used to obtain ordinary differential equations for the amplitudes in v.

Equation (15) generalizes for three-dimensional equilibria the definition of the toroidal angle used by Grimm, Dewar, and Manickam[4] for axisymmetric systems. The procedure of varying the toroidal angle ζ, which is a natural extension of our earlier work, is equivalent to the procedure used by Bauer, Betancourt, and Garabedian[5], and more recently, by Hirshman and Whitson.[6] It has the attractive feature that the equilibrium constraint embodied by Eq. (4) is satisfied throughout the plasma volume at every step of the iteration process.

The plan of the paper is as follows. In Sec. II, we describe the variational principle and derive the relevant Euler-Lagrange equations. In Sec. III, we expand R, Z, and Λ in Fourier series and derive from the variational principle Euler-Lagrange equations for the amplitudes in v. In Sec. IV, we explain our choice of the radial label, the boundary conditions, and explain the modifications necessary in our earlier code in order to accommodate variation of ζ. In Sec. V, we report comparisons with the analytic Solov'ev equilibria used to benchmark the earlier version of our code, and numerical results on three-dimensional stellarator equilibria.

II. VARIATIONAL PRINCIPLE

It has been shown[1,2] that the first variation of the functional

$$L = \int_{V_0} d\tau \left(\frac{B^2}{2} - p \right) , \tag{6}$$

defined over the total volume V_0 of a toroidal plasma bounded by a perfectly conducting wall, with $\underset{\sim}{B}$ represented by Eq. (2) and pressure $p = p(v)$, vanishes if, and only if, the magnetostatic equations are satisfied. Treating $R(v,\theta,\zeta)$, $Z(v,\theta,\zeta)$ and $\Lambda(v,\theta,\zeta)$ as dependent variables, we write L in the form

$$L \equiv \int_0^a dv \int_0^{2\pi} d\theta \int_0^{2\pi} d\zeta \; \mathscr{L}(R, R_v, R_\theta, R_\zeta, Z_v, Z_\theta, Z_\zeta, \Lambda_\theta, \Lambda_\zeta) ,$$

$$= \int_0^a dv \int_0^{2\pi} d\theta \int_0^{2\pi} d\zeta \; \sqrt{\| g \|} \left(\frac{\alpha_v^2}{2} \frac{g_{\theta\theta}}{\| g \|} + \frac{\beta_v^2}{2} \frac{g_{\zeta\zeta}}{\| g \|} + \alpha_v \beta_v \frac{g_{\theta\zeta}}{\| g \|} - p \right) , \tag{7}$$

where

$$\alpha_v \equiv \Psi_v (1 - q\Lambda_\zeta) , \tag{8a}$$

and

$$\beta_v \equiv \Phi_v (1 + \Lambda_\theta) . \tag{8b}$$

The elements of the metric tensor g_{ij} are given by

$$g_{vv} = R_v^2 + Z_v^2 , \tag{9a}$$

$$g_{v\theta} = R_v R_\theta + Z_v Z_\theta = g_{\theta v} \ , \tag{9b}$$

$$g_{\zeta v} = R_\zeta R_v + Z_\zeta Z_v = g_{v\zeta} \ , \tag{9c}$$

$$g_{\theta\theta} = R_\theta^2 + Z_\theta^2 \ , \tag{9d}$$

$$g_{\theta\zeta} = R_\theta R_\zeta + Z_\theta Z_\zeta = g_{\zeta\theta} \ , \tag{9e}$$

$$g_{\zeta\zeta} = R^2 + R_\zeta^2 + Z_\zeta^2 \ , \tag{9f}$$

and the Jacobian

$$\sqrt{\| g \|} = R(R_\theta Z_v - R_v Z_\theta) \ . \tag{10}$$

Two comments are in order. First, the form of $\mathscr{L}_I$ given by Eq. (7) is identical to the form given in Ref. 1 if we replace α_v by Ψ_v, and β_v by Φ_v. This observation helps us carry over most of the algebraic manipulations in Ref. 1 easily. Second, $\mathscr{L}_I$ is independent of Λ_v. The Euler-Lagrange equation for Λ is therefore expected to be independent of Λ_v, and may be solved within each magnetic surface.

The first variation of L gives, in the manner shown in Ref. 1, the following Euler-Lagrange equations for variations with respect to R, Z, and Λ respectively:

$$Q_1 \equiv \left(RZ_\theta \frac{\partial}{\partial v} - RZ_v \frac{\partial}{\partial \theta}\right)\left(\frac{\alpha_v^2}{2}\frac{g_{\theta\theta}}{\|g\|} + \frac{\beta_v^2}{2}\frac{g_{\zeta\zeta}}{\|g\|} + \alpha_v\beta_v \frac{g_{\theta\zeta}}{\|g\|} + p\right)$$

$$+ \alpha_v^2 \frac{\partial}{\partial\theta}\frac{R_\theta}{\sqrt{\|g\|}} + \beta_v^2\left(\frac{\partial}{\partial\zeta}\frac{R_\zeta}{\sqrt{\|g\|}} - \frac{R}{\sqrt{\|g\|}}\right) + \alpha_v\beta_v\left(\frac{\partial}{\partial\theta}\frac{R_\zeta}{\sqrt{\|g\|}} + \frac{\partial}{\partial\zeta}\frac{R_\theta}{\sqrt{\|g\|}}\right)$$

$$= 0 \qquad (11)$$

$$Q_3 \equiv \left(-RR_\theta \frac{\partial}{\partial v} + RR_v \frac{\partial}{\partial\theta}\right)\left(\frac{\alpha_v^2}{2}\frac{g_{\theta\theta}}{\|g\|} + \frac{\beta_v^2}{2}\frac{g_{\zeta\zeta}}{\|g\|} + \alpha_v\beta_v\frac{g_{\theta\zeta}}{\|g\|} + p\right)$$

$$+ \alpha_v^2\frac{\partial}{\partial\theta}\frac{Z_\theta}{\sqrt{\|g\|}} + \beta_v^2\frac{\partial}{\partial\zeta}\frac{Z_\zeta}{\sqrt{\|g\|}} + \alpha_v\beta_v\left(\frac{\partial}{\partial\theta}\frac{Z_\zeta}{\sqrt{\|g\|}} + \frac{\partial}{\partial\zeta}\frac{Z_\theta}{\sqrt{\|g\|}}\right) = 0 \ , \qquad (12)$$

and

$$Q_0 \equiv \frac{\partial}{\partial\theta}\left\{\frac{\Phi_v}{\sqrt{\|g\|}}\left[g_{\zeta\zeta}(\Lambda_\theta + 1) - g_{\theta\zeta}\Lambda_\zeta\right] + \frac{\Psi_v}{\sqrt{\|g\|}}g_{\theta\zeta}\right\}$$

$$- \frac{\partial}{\partial\zeta}\left\{\frac{\Phi_v}{\sqrt{\|g\|}}\left[g_{\theta\zeta}(\Lambda_\theta + 1) - g_{\theta\theta}\Lambda_\zeta\right] + \frac{\Psi_v}{\sqrt{\|g\|}}g_{\theta\theta}\right\} = 0 \ . \qquad (13)$$

Equations (11), (12) and (13) may be identified to be

$$\underset{\sim}{\nabla}R\cdot\underset{\sim}{\nabla}\left(\frac{B^2}{2} + p\right) - \underset{\sim}{B}\cdot\underset{\sim}{\nabla}B_R - \frac{B_\phi^2}{R} = 0 \ , \qquad (14)$$

$$\underset{\sim}{\nabla}Z\cdot\underset{\sim}{\nabla}\left(\frac{B^2}{2} + p\right) - \underset{\sim}{B}\cdot\underset{\sim}{\nabla}(B_Z) = 0 \ , \qquad (15)$$

and

$$\underset{\sim}{J}\cdot\underset{\sim}{\nabla}v \;=\; \underset{\sim}{\nabla}\cdot(\underset{\sim}{B}\times\underset{\sim}{\nabla}v) \;=\; 0 \quad , \tag{16}$$

respectively, where

$$B_R \;\equiv\; \underset{\sim}{B}\cdot\underset{\sim}{\nabla}R \quad , \tag{17a}$$

$$B_\phi \;\equiv\; R\underset{\sim}{B}\cdot\underset{\sim}{\nabla}\phi \quad , \tag{17b}$$

and

$$B_Z \;\equiv\; \underset{\sim}{B}\cdot\underset{\sim}{\nabla}Z \quad . \tag{17c}$$

Equations (14) and (15) are, respectively, the covariant components in the $\underset{\sim}{\nabla}R$ and $\underset{\sim}{\nabla}Z$ directions of $\underset{\sim}{J}\times\underset{\sim}{B} = \underset{\sim}{\nabla}p$, which may be written in the form

$$\underset{\sim}{\nabla}\left(\frac{B^2}{2} + p\right) - \underset{\sim}{B}\cdot\underset{\sim}{\nabla}\underset{\sim}{B} \;=\; 0 \quad . \tag{18}$$

As pointed out in Ref. 1, the covariant component of Eq. (18) in the $\underset{\sim}{\nabla}\phi$ direction,

$$R\underset{\sim}{\nabla}\phi\cdot\underset{\sim}{\nabla}\left(\frac{B^2}{2} + p\right) - \underset{\sim}{B}\cdot\underset{\sim}{\nabla}(RB_\phi) \;=\; 0 \tag{19}$$

may be shown to be a consequence of Eqs. (14), (15) and (16) and is not an independent equation.

Before we conclude this section, we write for future reference, $\underset{\sim}{J}\times\underset{\sim}{B} = p_v\underset{\sim}{\nabla}v$, in terms of inverse variables R and Z , and Λ :

$$Q \equiv \frac{\alpha_v}{\sqrt{\|g\|}}\left[\frac{\partial}{\partial v}\left(\frac{\alpha_v g_{\theta\theta}}{\sqrt{\|g\|}} + \frac{\beta_v g_{\theta\zeta}}{\sqrt{\|g\|}}\right) - \frac{\partial}{\partial\theta}\left(\frac{\alpha_v g_{v\theta}}{\sqrt{\|g\|}} + \frac{\beta_v g_{\zeta v}}{\sqrt{\|g\|}}\right)\right]$$

$$+ \frac{\beta_v}{\sqrt{\|g\|}}\left[\frac{\partial}{\partial v}\left(\frac{\alpha_v g_{\theta\zeta}}{\sqrt{\|g\|}} + \frac{\beta_v g_{\zeta\zeta}}{\sqrt{\|g\|}}\right) - \frac{\partial}{\partial\zeta}\left(\frac{\alpha_v g_{v\theta}}{\sqrt{\|g\|}} + \frac{\beta_v g_{\zeta v}}{\sqrt{\|g\|}}\right)\right] + p_v = 0 \quad . \qquad (20)$$

III. EULER-LAGRANGE EQUATIONS FOR FOURIER AMPLITUDES

Exploiting the periodicity of $R(v,\theta,\zeta)$, $Z(v,\theta,\zeta)$ and $\Lambda(v,\theta,\zeta)$ in θ and ζ , we expand them in Fourier series.

$$R(v,\theta,\zeta) = \sum\left[R_{m_1,m_2}(v)\cos(m_1\theta - m_2\zeta) + R_{n_1,n_2}(v)\sin(n_1\theta - n_2\zeta)\right] \qquad (21)$$

$$Z(v,\theta,\zeta) = \sum\left[Z_{p_1,p_2}(v)\cos(p_1\theta - p_2\zeta) + Z_{q_1,q_2}(v)\sin(q_1\theta - q_2\zeta)\right] \qquad (22)$$

$$\Lambda(v,\theta,\zeta) = \sum\left[\Lambda_{r_1,r_2}(v)\cos(r_1\theta - r_2\zeta) + \Lambda_{s_1,s_2}(v)\sin(s_1\theta - s_2\zeta)\right] \qquad (23)$$

where, unless stated otherwise, the sums extend from $-\infty$ to $+\infty$ over all integers. Substituting series (21) through (23) in L , and varying

each amplitude in v independently, we derive the following infinite set of ordinary differential equations for stationary values of L :

$$\langle\langle \cos(m_1\theta - m_2\zeta)Q_1 \rangle\rangle = 0 \qquad m_1, m_2 \in (-\infty, +\infty) \tag{24a}$$

$$\langle\langle \sin(n_1\theta - n_2\zeta)Q_1 \rangle\rangle = 0 \qquad n_1, n_2 \in (-\infty, +\infty) \tag{24b}$$

$$\langle\langle \cos(p_1\theta - p_2\zeta)Q_3 \rangle\rangle = 0 \qquad p_1, p_2 \in (-\infty, +\infty) \tag{24c}$$

$$\langle\langle \sin(q_1\theta - q_2\zeta)Q_3 \rangle\rangle = 0 \qquad q_1, q_2 \in (-\infty, +\infty) \tag{24d}$$

$$\langle\langle \cos(r_1\theta - r_2\zeta)Q_0 \rangle\rangle = 0 \qquad r_1, r_2 \in (-\infty, +\infty) \tag{24e}$$

$$\langle\langle \sin(s_1\theta - s_2\zeta)Q_0 \rangle\rangle = 0 \qquad s_1, s_2 \in (-\infty, +\infty) \tag{24f}$$

where $\langle\langle\ \rangle\rangle$ is the double-averaging operator, defined by

$$\langle\langle A \rangle\rangle \equiv (2\pi)^{-2} \int_0^{2\pi} d\theta \int_0^{2\pi} d\zeta\ A(v,\theta,\zeta) \quad . \tag{25}$$

In what follows we will consider equilibria which have the symmetry property that if $\theta \to -\theta$ and $\zeta \to -\zeta$, then $R \to R$ and $Z \to -Z$. The above symmetry operations require that $\Lambda \to -\Lambda$. We will, therefore, restrict ourselves to only Eqs. (24a), (24d) and (24f).

IV. CHOICE OF THE RADIAL FLUX SURFACE LABEL AND BOUNDARY CONDITIONS

As pointed out in Ref. 1, any one of the Fourier amplitudes may be used for labelling flux surfaces. The surface-averaged pressure balance equation, given by

$$\left\langle\left\langle \sqrt{\| g \|}\; Q \right\rangle\right\rangle = 0 \quad , \tag{26}$$

takes the place, formally speaking, of the Euler-Lagrange equation for the Fourier amplitude chosen. Alternatively, we may specify the functional relation between v and Ψ ,

$$v = v(\Psi) \quad . \tag{27}$$

Following the practice of Ref. 1, we continue to use $R_{10} = -|\alpha| v$, where $|\alpha|$ is a positive scaling factor fixed by the geometry of the outermost surface.

One set of boundary conditions for the Fourier amplitudes is obtained by Fourier analyzing the outermost surface at $v = a$. We define

$$R^a_{m_1,m_2} \equiv R_{m_1,m_2}(a) \quad , \tag{28a}$$

$$Z^a_{q_1,q_2} \equiv Z_{q_1,q_2}(a) \quad . \tag{28b}$$

The poloidal flux function Ψ is a constant on the outermost surface, given by

$$\Psi^a \equiv \Psi(a) \quad . \tag{29}$$

Near the axis we impose, as in Ref. 1,

$$R'_{m_1,m_2}(0) = 0 \qquad (m_1 = 0) \quad , \tag{30a}$$

$$R_{m_1,m_2}(0) = 0 \qquad (m_1 \neq 0) \quad , \tag{30b}$$

$$Z'_{q_1,q_2}(0) = 0 \qquad (q_1 = 0) \ , \tag{30c}$$

$$Z_{q_1,q_2}(0) = 0 \qquad (q_1 \neq 0) \ , \tag{30d}$$

where $f' \equiv f_v$.

The boundary condition for Ψ at $v = 0$, necessary in order to pin down the solution to Eq. (20), needs to be handled carefully. In the manner shown in Ref. 1, we transform to a new dependent variable

$$u(v) = \frac{\Psi_v}{v} \ , \tag{31}$$

and use the transformed Eq. (20) to obtain $u(0)$ iteratively. Once u is obtained, we integrate Eq. (31), subject to Eq. (29), to obtain Ψ .

The moment equations for Λ , given by Eq. (24f), have no radial derivatives, and are therefore solved within each surface. The numerical results we present are determined by two given functions, the toroidal field function $F(\Psi)$ and the pressure $p(\Psi)$. In the special case of axisymmetry

$$F = \Phi_v \frac{g_{\zeta\zeta}}{\sqrt{\| g \|}} (1 + \Lambda_\theta) \ . \tag{32}$$

The solubility condition for Λ now gives

$$F = \frac{\Phi_v}{\langle\langle \sqrt{\| g \|} / g_{\zeta\zeta} \rangle\rangle} \ , \tag{33}$$

which is subtly different from the prescription for F in Ref. 1.

Though introduced here in the context of axisymmetry, we carry over the prescription given by Eq. (33) for three-dimensional equilibria. To obtain Φ , we integrate Eq. (33) subject to the condition

$$\Phi(0) = 0 \quad . \tag{34}$$

In summary, we solve numerically Eqs. (24a), (24d), (24f), (26) and (33), subject to the stated boundary conditions, by the method of collocation at Gaussian points due to DeBoor and Swartz.[7] For a detailed explanation, the reader is referred to Ref. 1. We state here only the modification due to the introduction of Λ in the formalism. The moment equations for Λ , given by Eq. (24f), have no radial derivatives, and are therefore solved within each surface at every step of the iteration process. This may not be the most computationally efficient strategy, because it does not sufficiently exploit the fact that Q_0 is a linear, Poisson-like equation in Λ . However, we have adopted it because it was the easiest one to implement within the existing framework of our earlier code.

V. NUMERICAL RESULTS

We first compare the numerical results with the analytic, axisymmetric Solov́ev equilibrium used as a test case in Ref. 1. The outermost surface is described by the parametric equations

$$R(v=a,\theta) = R^a_{00} - |\alpha|\cos\theta + R^a_{20}\cos 2\theta + R^a_{30}\cos 3\theta \tag{35a}$$

and

$$Z(v=a,\theta) = Z^a_{10}\sin\theta + Z^a_{20}\sin 2\theta + Z^a_{30}\sin 3\theta \qquad (35b)$$

where $R^a_{00} = 3.881$, $|\alpha| = 1.036$, $R^a_{20} = -0.0172$, $R^a_{30} = 1.8\times 10^{-4}$, $Z^a_{10} = 1.569$, $Z^a_{20} = 0.0807$, and $Z^a_{30} = -3.89\times 10^{-3}$. In Fig. 1, we show the flux surface contours on any poloidal section of the torus. In Fig. 2, we show the radial profiles of the dominant Fourier amplitudes. On comparison with the analogous plot in Ref. 1, we no longer observe the "boundary-layer" effect, noticable, for example, in R_{00} R_{30} , and Z_{30} of Fig. 3 in Ref. 1.

In Table I, we compare the error in Ψ (defined to be $\max|\Psi^N - \Psi|/\Psi^a$, where Ψ^N and Ψ are respectively the numerical and exact values of Ψ as we increase the number of splines (or collocation points), holding all other parameters fixed. There is considerable improvement over our earlier results not only in the absolute magnitude of the error, but more importantly, in the rate of convergence.

We now present numerical results on the three-dimensional equilibria reported in Ref. 1. For the first case, the outermost surface is given by

$$R = R^a_{00} - |\alpha|\cos\theta + R^a_{20}\cos 2\theta + R^a_{11}\cos(\theta - \zeta) \qquad (36a)$$

$$Z = Z^a_{10}\sin\theta + Z^a_{20}\sin 2\theta + Z^a_{11}\sin(\theta - \zeta) \ , \qquad (36b)$$

where R^a_{00} , $|\alpha|$, R^a_{20} , Z^a_{10} , and Z^a_{20} have the same numerical values as Eqs. (35), and $R^a_{11} = Z^a_{11} = 0.333$. In Fig. 4, we show the flux surface contours on different poloidal planes along the axis and in

Fig. 5 the radial profiles of the dominant Fourier amplitudes. The magnetic axis for this equilibrium lies almost entirely in a plane.

We then consider a three-dimensional equilibrium with a spatial magnetic axis. The outermost surface is described by

$$R = R^a_{00} - |\alpha|\cos\theta + R^a_{20}\cos 2\theta + R^a_{01}\cos\zeta \qquad (37a)$$

$$Z = Z^a_{10}\sin\theta + Z^a_{20}\sin 2\theta + Z^a_{01}\sin\zeta \quad , \qquad (37b)$$

where once again R^a_{00} , $|\alpha|$, R^a_{20} , Z^a_{10} , and Z^a_{20} have the same numerical values as before and $R^a_{01} = Z^a_{01} = 0.333$. In Fig. 6, we show the flux surface contours, and in Fig. 7, the radial profiles for the dominant Fourier amplitudes.

In all the numerical results reported, we have used single precision arithmetic on a VAX-11/780 computer. The residuals for the equations solved numerically were in the range $10^{-4} - 10^{-7}$ for the solutions presented at the termination of the computer runs.

Acknowledgments

The first author (A.B.) would like to thank Ms. K. S. Al-Sweilem for typing this manuscript at short notice. This work was supported primarily by the United States Department of Energy under contract no. DE-FG05-80ET-53088 with the Institute for Fusion Studies and contract no. DE-AC05-79ET-53036 with the Fusion Research Center.

References

1. A. Bhattacharjee, J. C. Wiley, and R. L. Dewar, Institute for Fusion Studies Report IFSR#48-R (University of Texas, Austin, 1983).

2. H. Grad, Phys. Fluids 7, 1283 (1964).

3. M. D. Kruskal and R. M. Kulsrud, Phys. Fluids 1, 265 (1958).

4. R. C. Grimm, R. L. Dewar, and J. Manickam, PPPL-1885 (Princeton Plasma Physics Laboratory, New Jersey, 1982).

5. F. Bauer, O. Betancourt, and P. Garabedian, A Computational Method in Plasma Physics (Springer-Verlag, New York, 1978).

6. S. P. Hirshman and J. C. Whitson, Proceedings of the 1983 Sherwood Theory Meeting, March 21-23, 1983 in Arlington, Va., Paper 3A3.

Figure Captions

Fig. 1 Flux surfaces for the test Solov́ev equilibrium, projected on a poloidal surface.

Fig. 2 Radial profiles of the dominant Fourier amplitudes for the equilibrium shown in Fig. 1.

Fig. 3 Energy (normalized) versus number of iterations for the test Solov́ev equilibrium.

Fig. 4 Flux contours for a three-dimensional stellarator equilibrium with a planar magnetic axis.

Fig. 5 Radial profiles of the dominant Fourier amplitudes for the equilibrium shown in Fig. 4.

Fig. 6 Flux surface contours for a three-dimensional stellarator equilibrium with a spatial magnetic axis.

Fig. 7 Radial profiles of the dominant fourier amplitudes for the equilibrium shown in Fig. 6.

Fig. 1

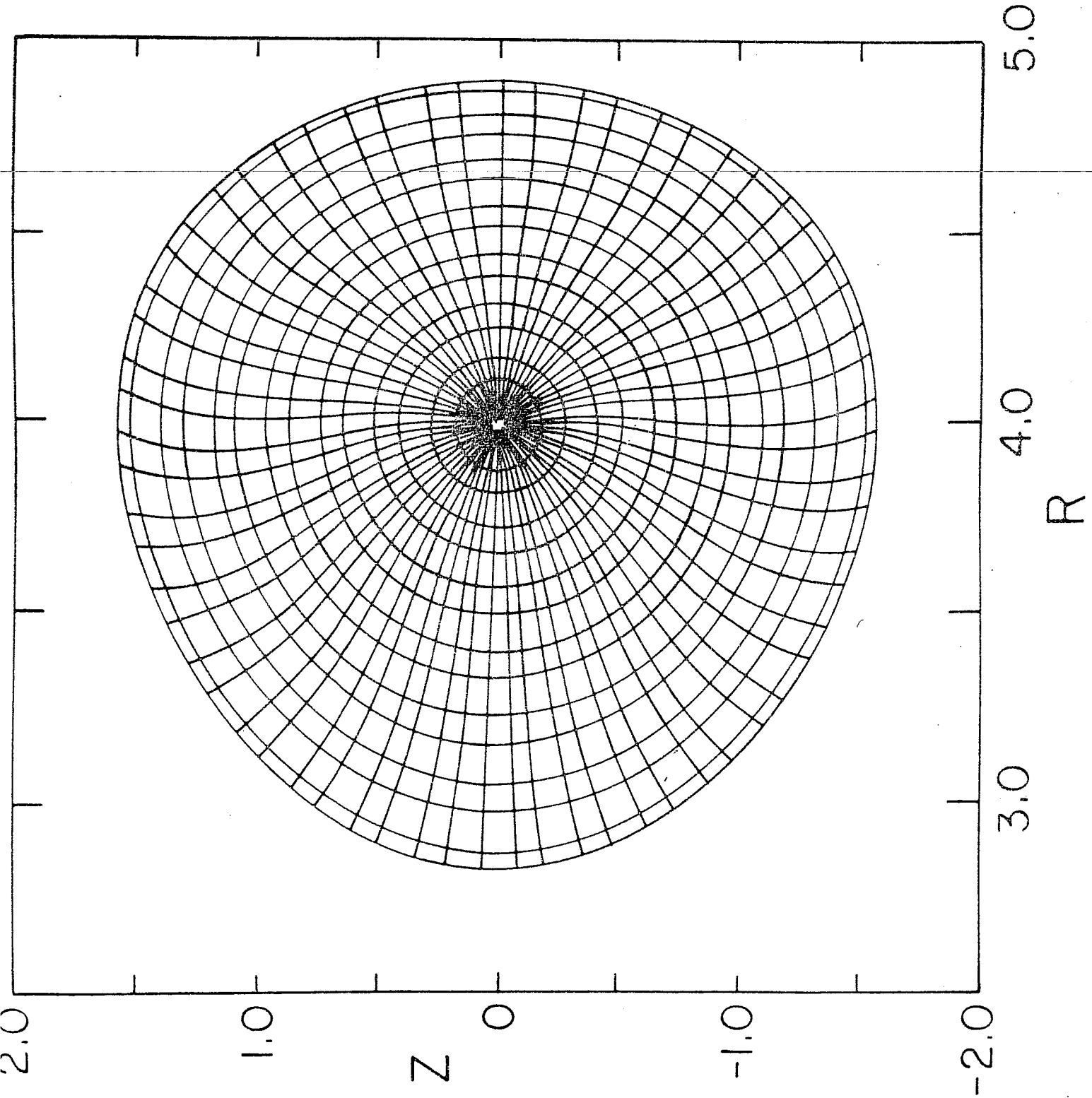

Fig. 2

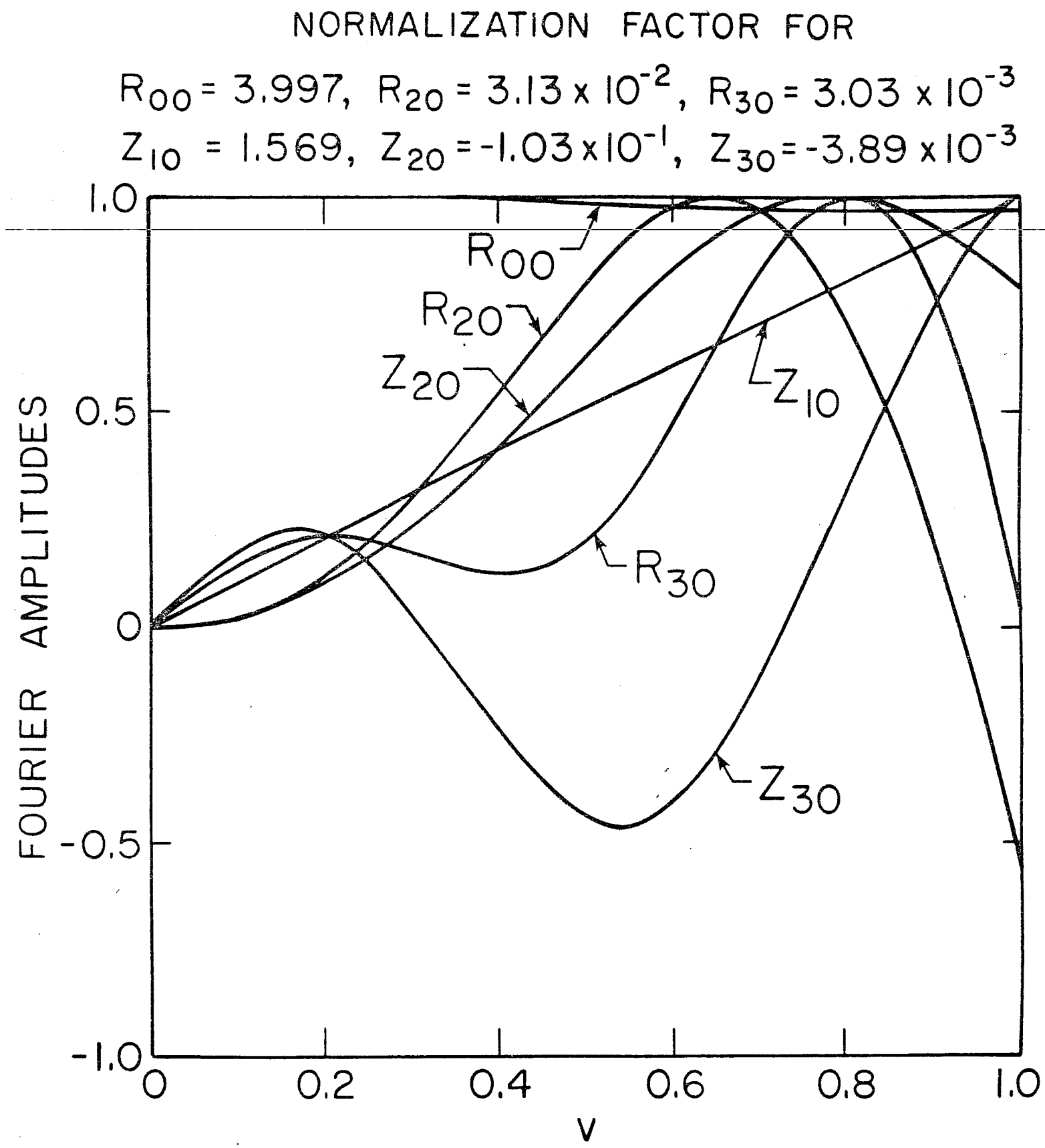
NORMALIZATION FACTOR FOR
$R_{00} = 3.997$, $R_{20} = 3.13 \times 10^{-2}$, $R_{30} = 3.03 \times 10^{-3}$
$Z_{10} = 1.569$, $Z_{20} = -1.03 \times 10^{-1}$, $Z_{30} = -3.89 \times 10^{-3}$
FOURIER AMPLITUDES
1.0
0.5
0
-0.5
-1.0
0
0.2
0.4
0.6
0.8
1.0
V
R_{00}
R_{20}
Z_{20}
Z_{10}
R_{30}
Z_{30}

Fig. 3

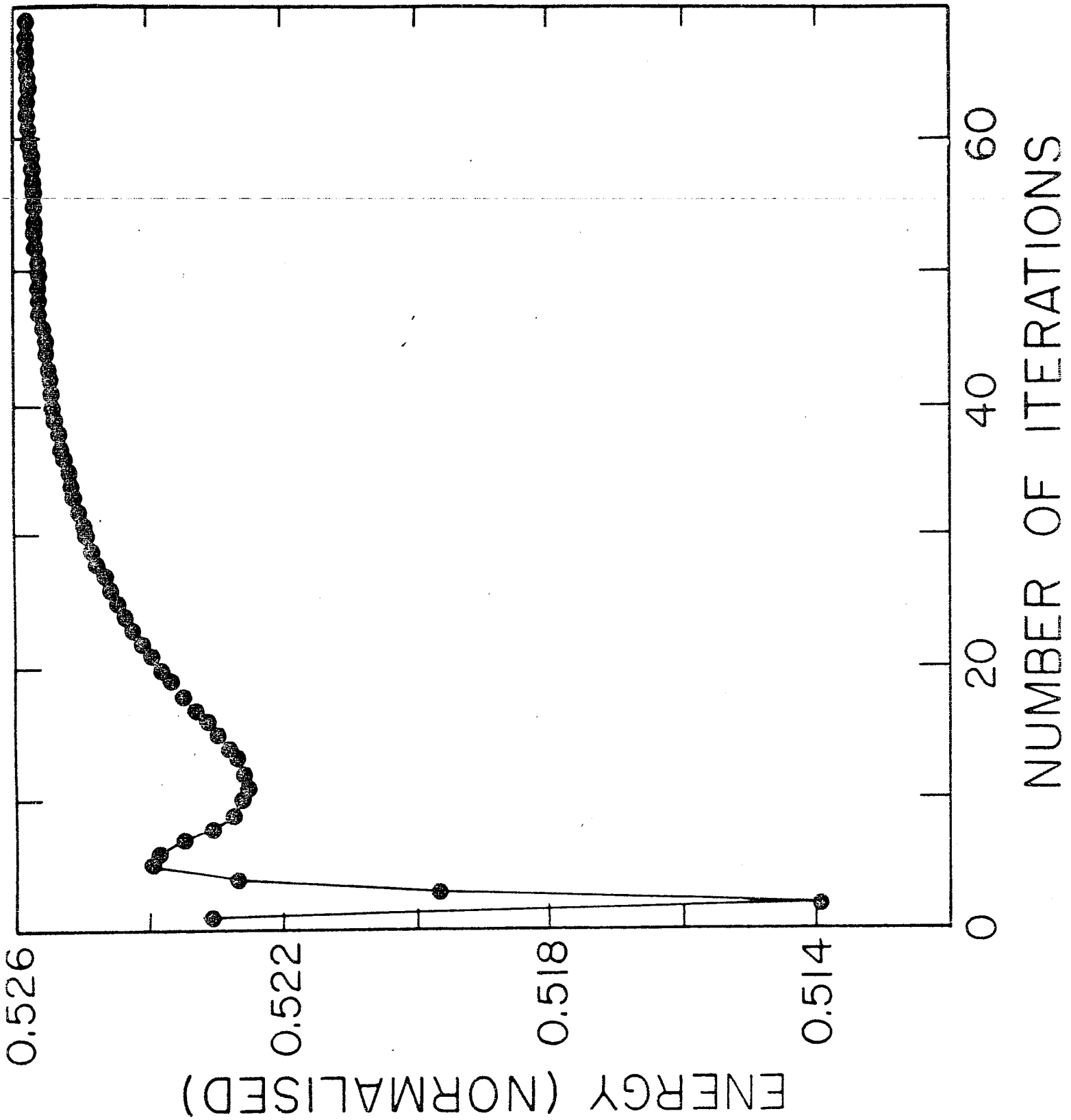
ENERGY (NORMALISED)
0.526
0.522
0.518
0.514
0
20
40
60
NUMBER OF ITERATIONS

Fig. 4

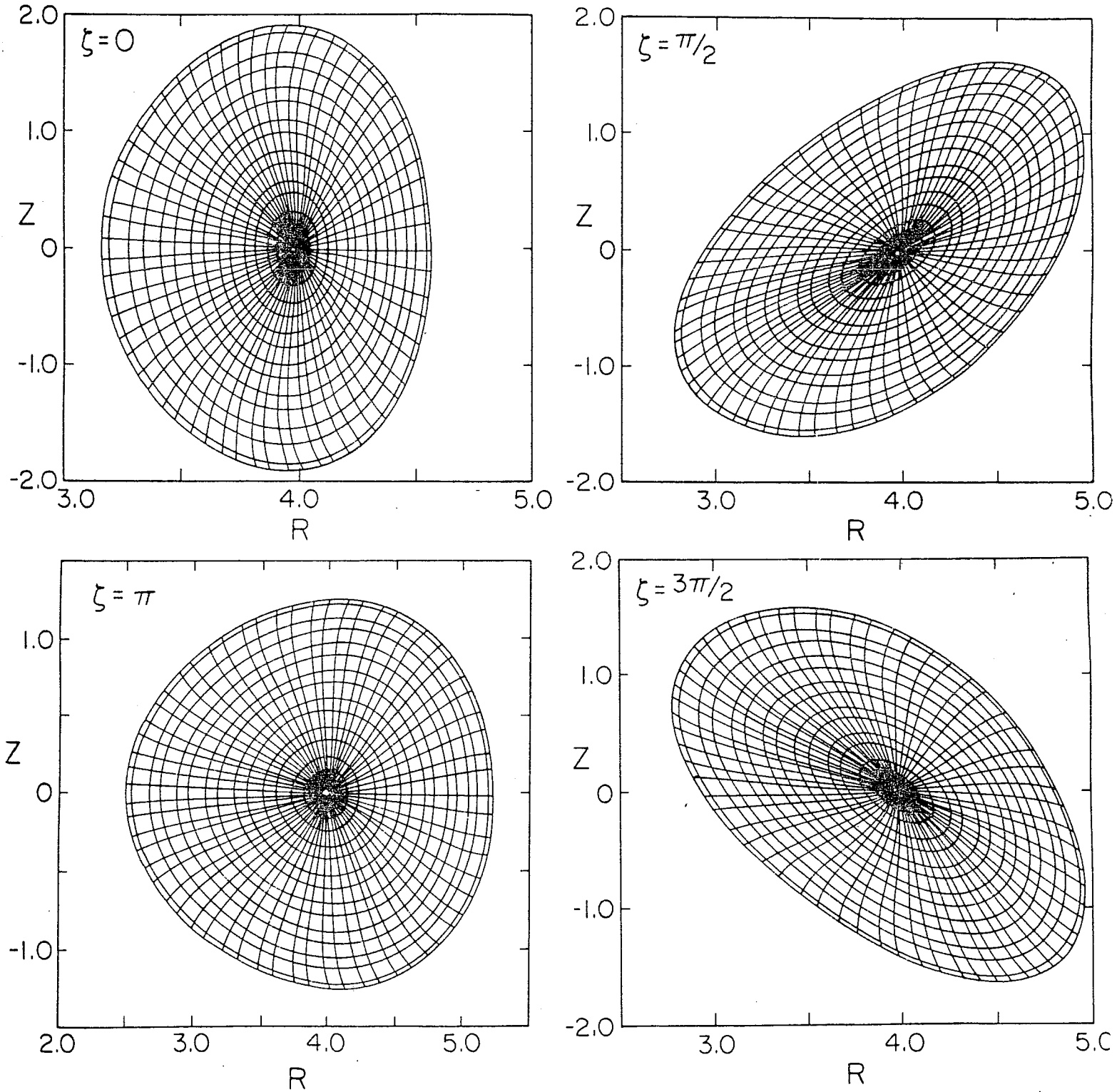

Fig. 5

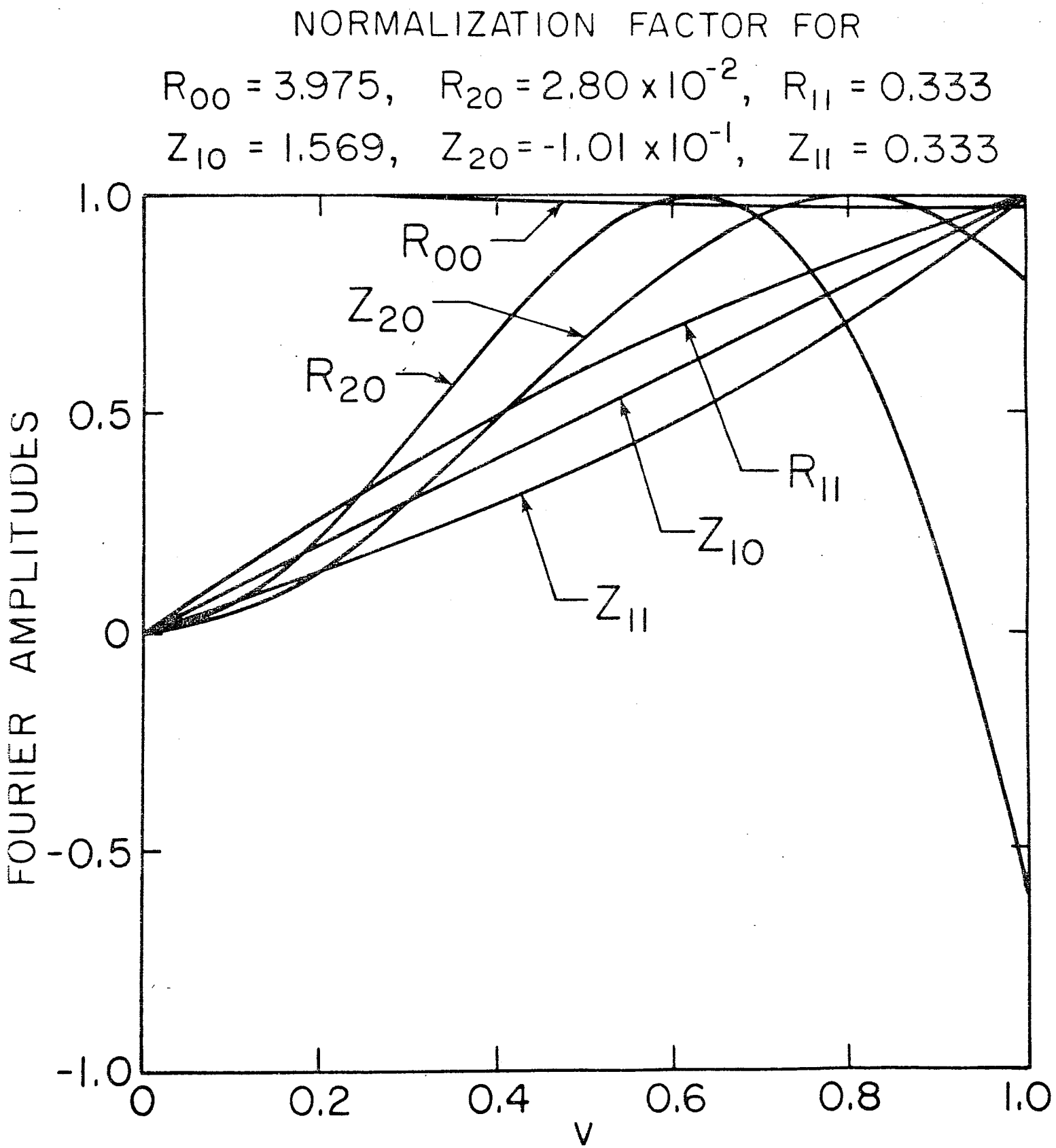
NORMALIZATION FACTOR FOR
$R_{00} = 3.975$, $R_{20} = 2.80 \times 10^{-2}$, $R_{11} = 0.333$
$Z_{10} = 1.569$, $Z_{20} = -1.01 \times 10^{-1}$, $Z_{11} = 0.333$
FOURIER AMPLITUDES
V
1.0
0.5
0
-0.5
-1.0
0
0.2
0.4
0.6
0.8
1.0
R_{00}
Z_{20}
R_{20}
R_{11}
Z_{10}
Z_{11}

Fig. 6

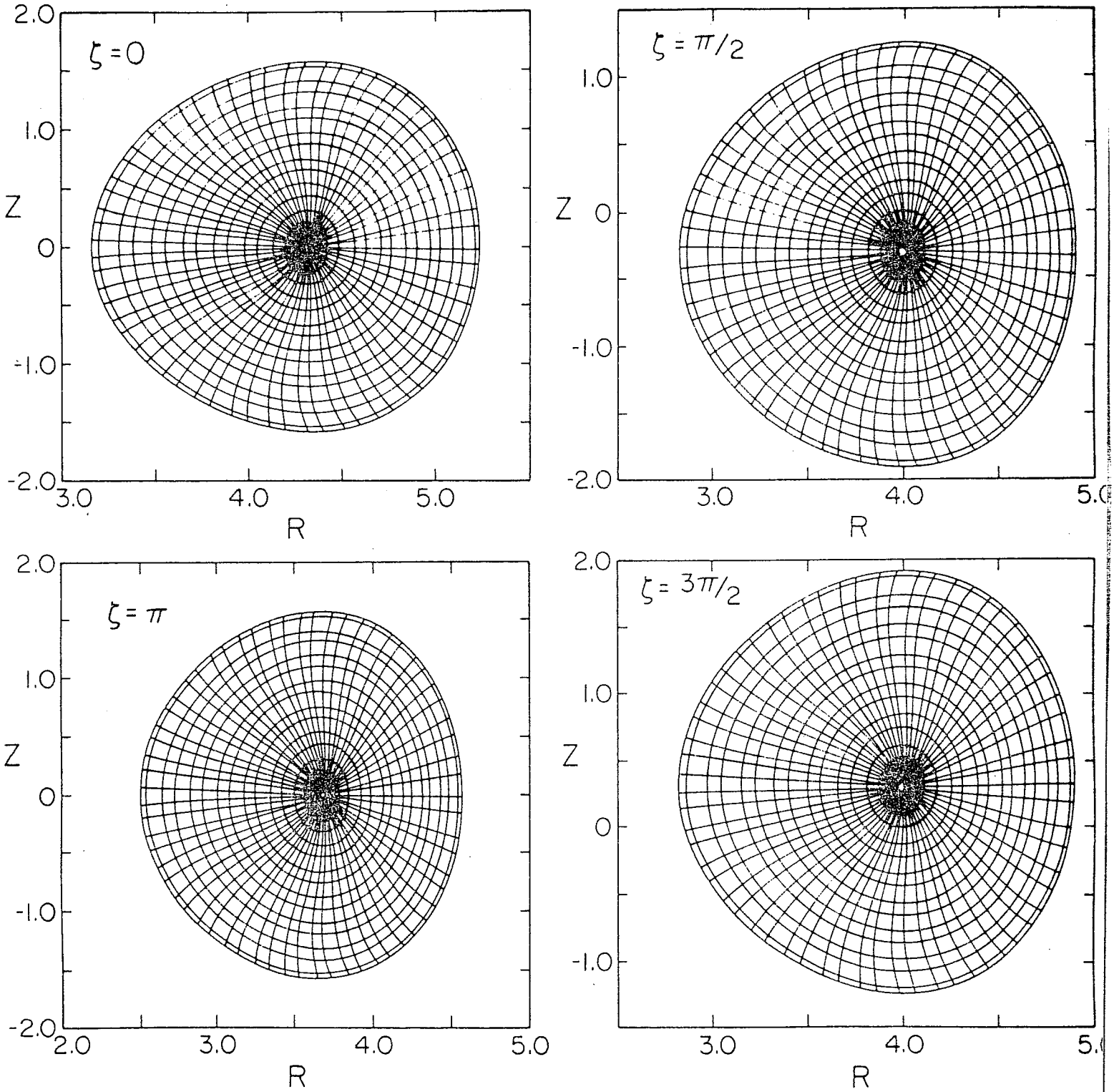

Fig. 7

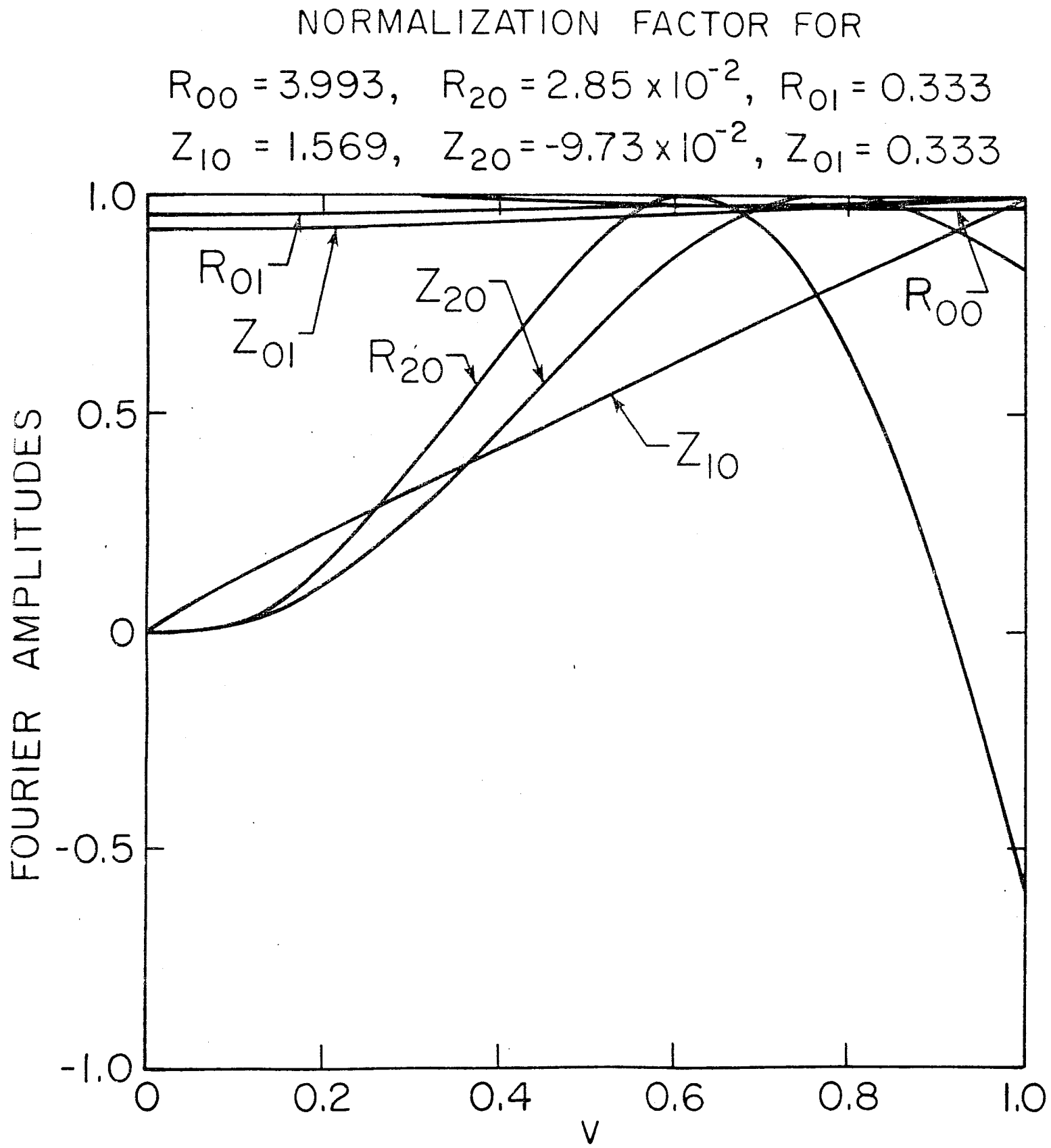
NORMALIZATION FACTOR FOR
$R_{00} = 3.993$, $R_{20} = 2.85 \times 10^{-2}$, $R_{01} = 0.333$
$Z_{10} = 1.569$, $Z_{20} = -9.73 \times 10^{-2}$, $Z_{01} = 0.333$
FOURIER AMPLITUDES
V
1.0
0.5
0
-0.5
-1.0
0
0.2
0.4
0.6
0.8
1.0
R_{01}
Z_{01}
Z_{20}
R_{20}
Z_{10}
R_{00}

Table I

Number of basis functions (N_s)	Number of collocation points (N_c)	Error $\equiv \max \dfrac{\lvert \psi^N - \psi \rvert}{\psi_a}$
8	6	9.03×10^{-3}
16	14	4.22×10^{-4}
32	30	5.74×10^{-5}

Error comparison for the test Solovev equilibrium for different choices of the number of basis functions (or collocation points).

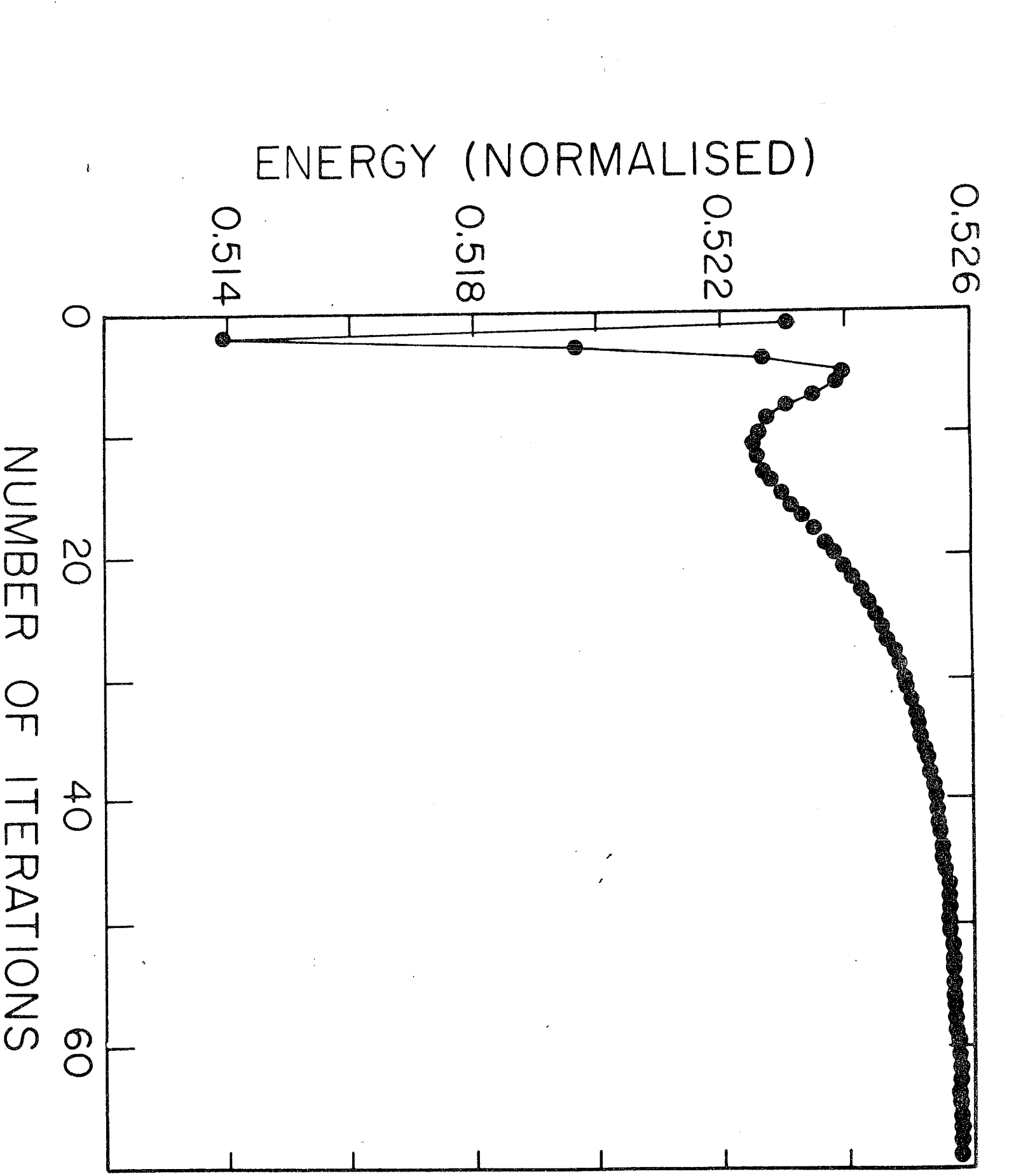
ENERGY (NORMALISED)
0.514
0.518
0.522
0.526
0
20
40
60
NUMBER OF ITERATIONS

Fig. 3

Table I

Number of basis functions (N_s)	Number of collocation points (N_c)	Error $\equiv \max\left\|\frac{\Psi^N - \Psi}{\Psi_a}\right\|$
8	6	9.03×10^{-3}
16	14	4.22×10^{-4}
32	30	5.74×10^{-5}

Error comparison for the test Solovev equilibrium for different choices of the number of basis functions (or collocation points).

Fig. 7

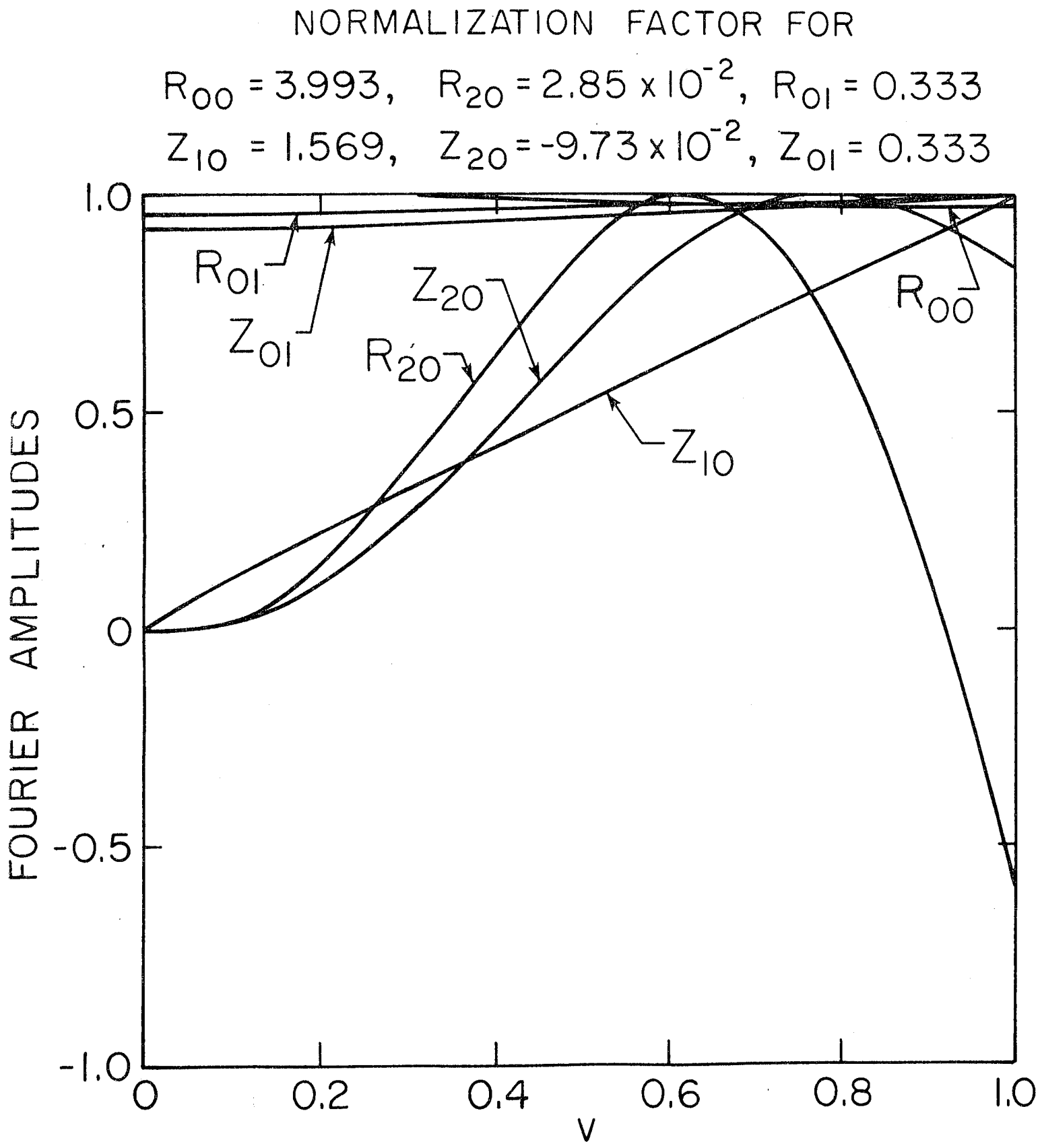
NORMALIZATION FACTOR FOR
$R_{00} = 3.993$, $R_{20} = 2.85 \times 10^{-2}$, $R_{01} = 0.333$
$Z_{10} = 1.569$, $Z_{20} = -9.73 \times 10^{-2}$, $Z_{01} = 0.333$
FOURIER AMPLITUDES
V
1.0
0.5
0
-0.5
-1.0
0
0.2
0.4
0.6
0.8
1.0
R_{01}
Z_{01}
Z_{20}
R_{20}
Z_{10}
R_{00}

Fig. 5

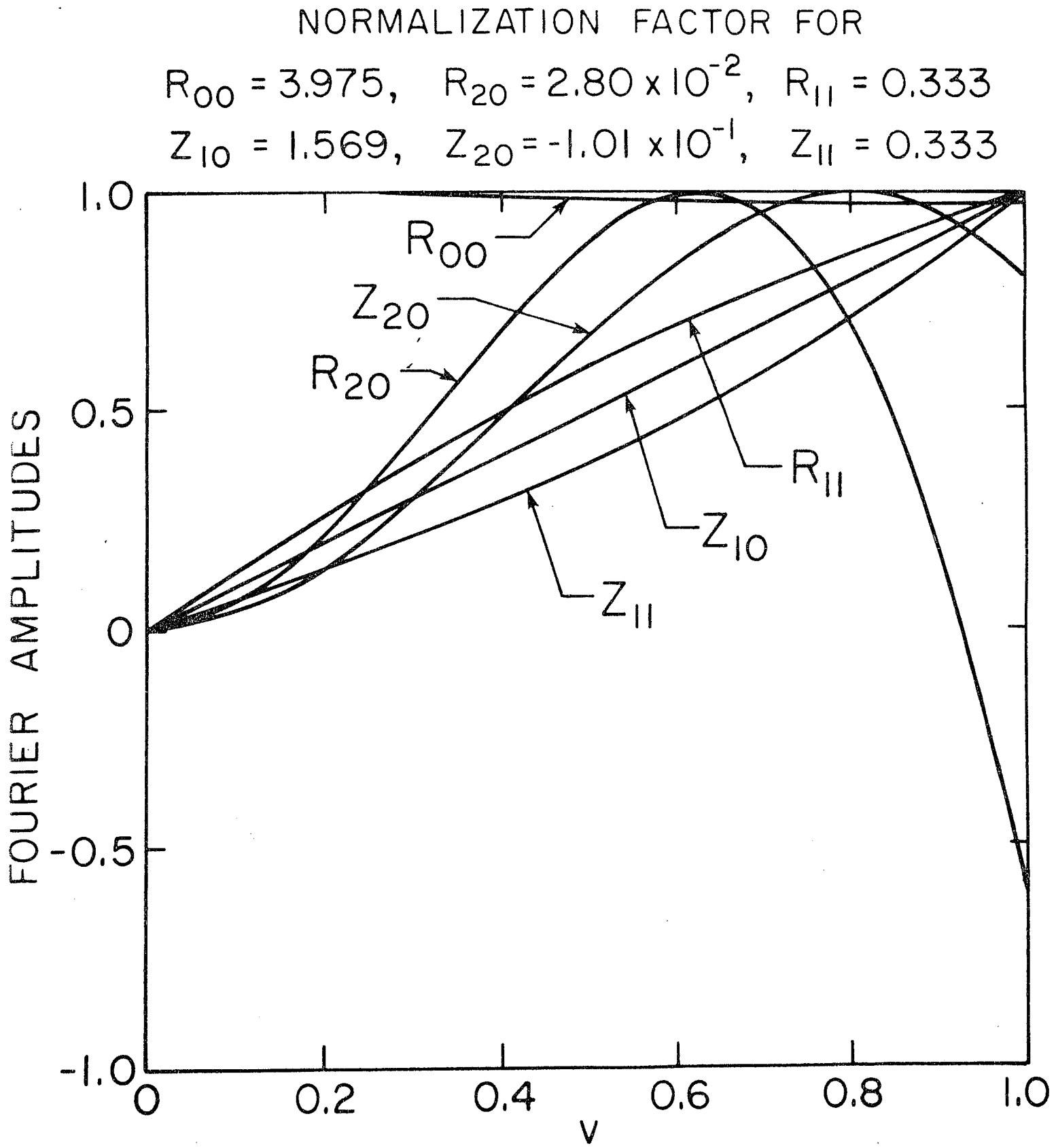
NORMALIZATION FACTOR FOR
$R_{00} = 3.975$, $R_{20} = 2.80 \times 10^{-2}$, $R_{11} = 0.333$
$Z_{10} = 1.569$, $Z_{20} = -1.01 \times 10^{-1}$, $Z_{11} = 0.333$
FOURIER AMPLITUDES
1.0
0.5
0
-0.5
-1.0
0
0.2
0.4
0.6
0.8
1.0
v
R_{00}
Z_{20}
R_{20}
R_{11}
Z_{10}
Z_{11}

Fig. 4

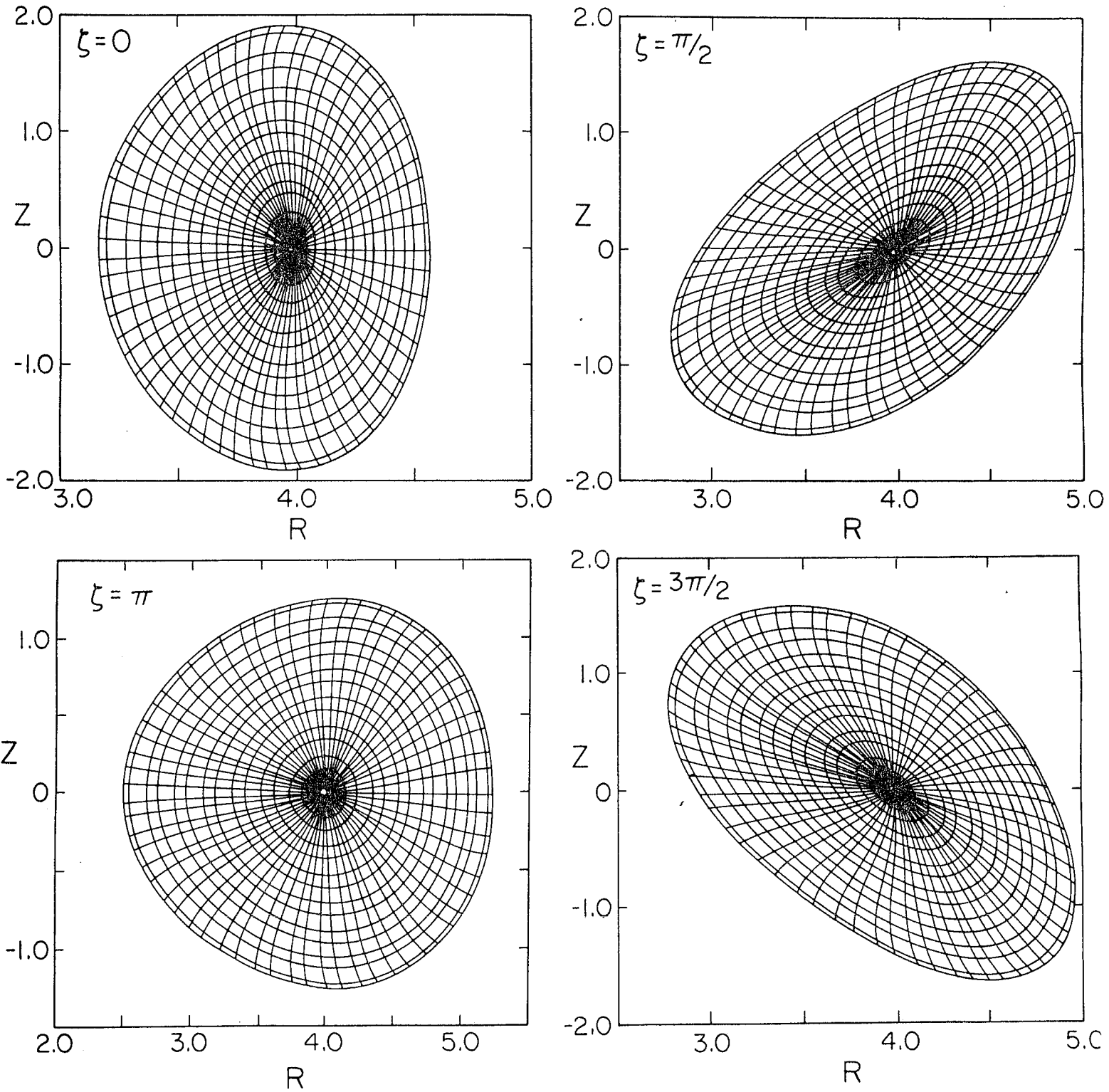

Fig. 6

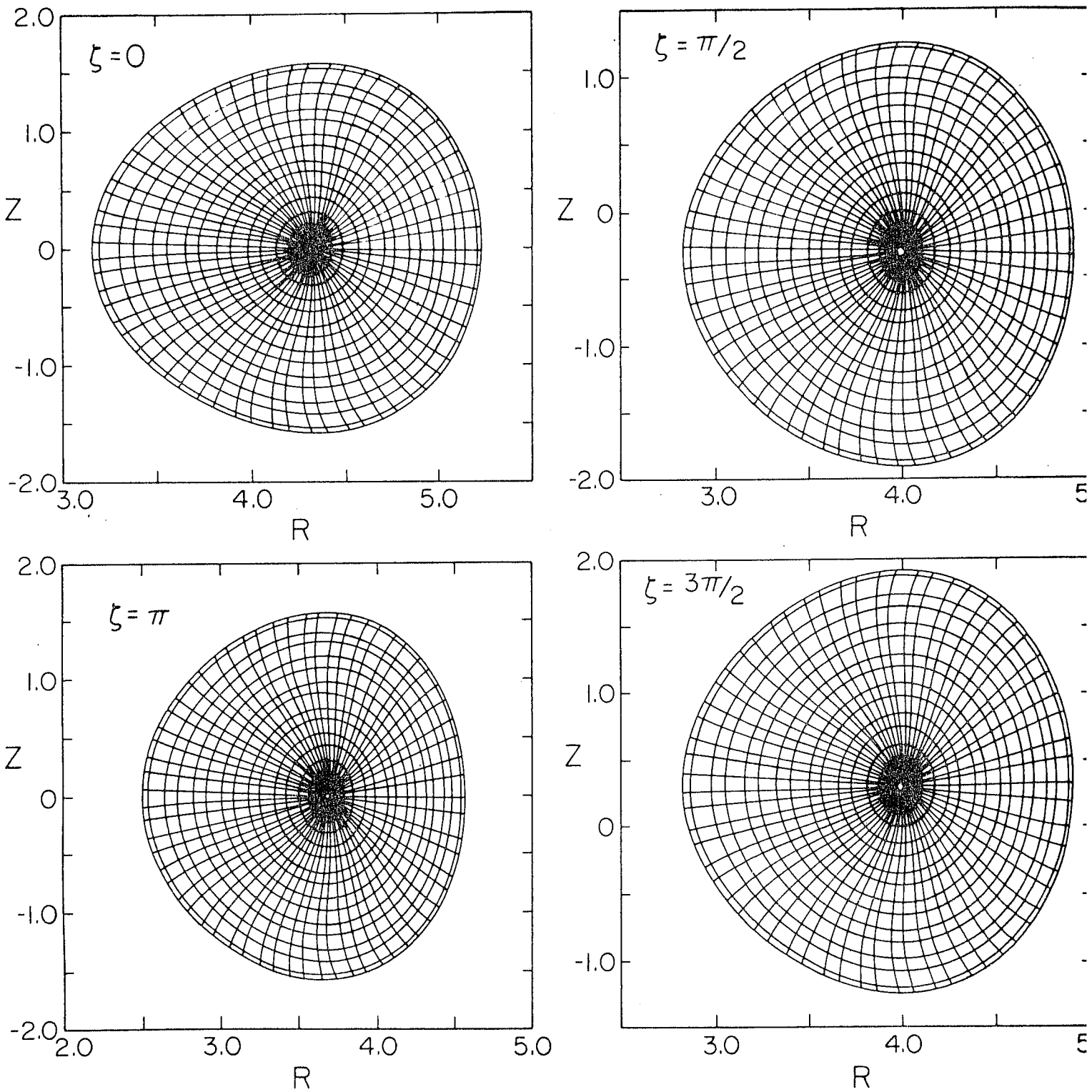

Fig. 2

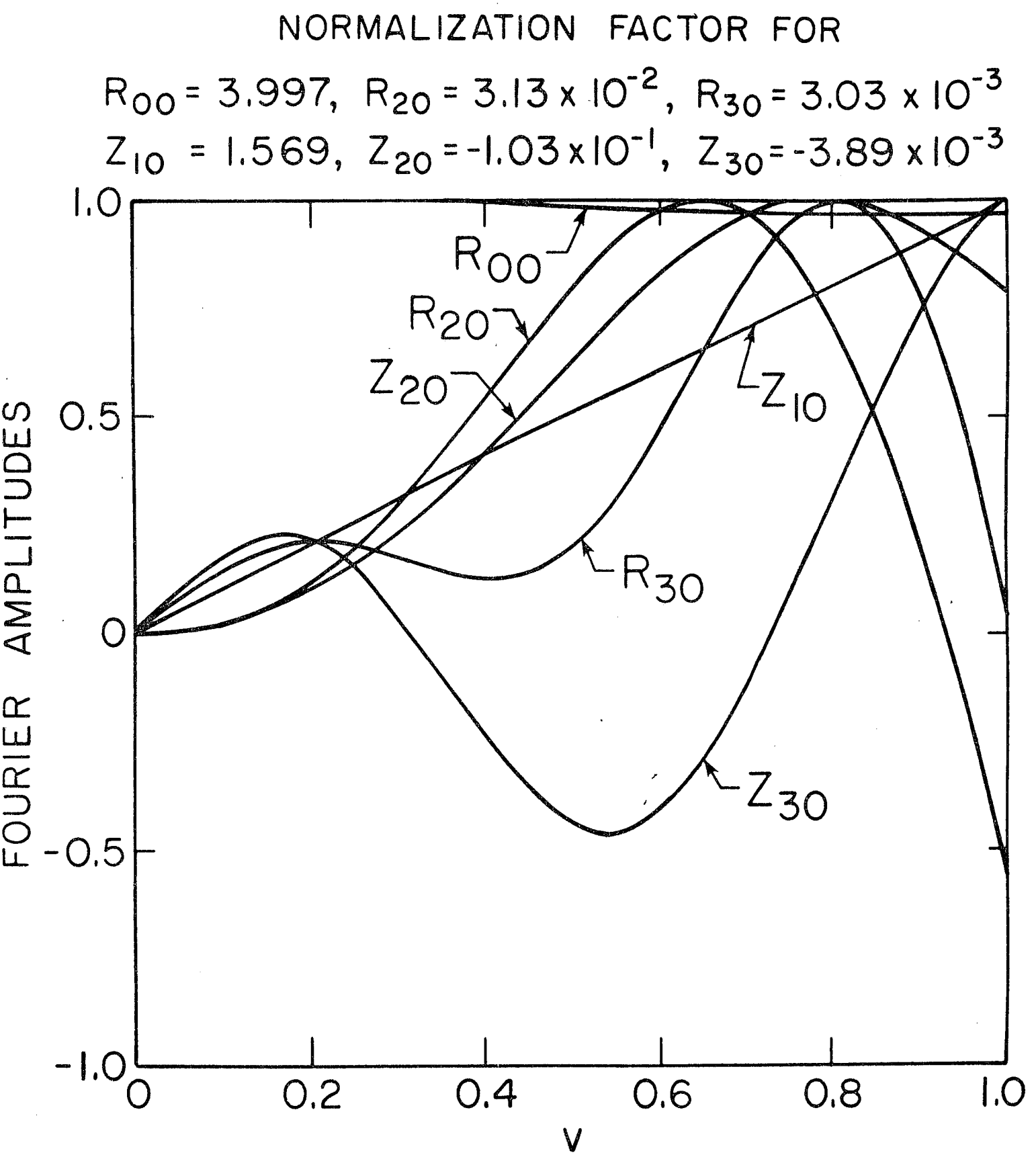
NORMALIZATION FACTOR FOR
$R_{00} = 3.997$, $R_{20} = 3.13 \times 10^{-2}$, $R_{30} = 3.03 \times 10^{-3}$
$Z_{10} = 1.569$, $Z_{20} = -1.03 \times 10^{-1}$, $Z_{30} = -3.89 \times 10^{-3}$
FOURIER AMPLITUDES
1.0
0.5
0
-0.5
-1.0
0
0.2
0.4
0.6
0.8
1.0
v
R_{00}
R_{20}
Z_{20}
Z_{10}
R_{30}
Z_{30}

Fig. 1